Structure of Large Nitrate−Water Clusters at Ambient Temperatures: Simulations with Effective Fragment Potentials and Force Fields with Implications for Atmospheric Chemistry

Yifat Miller,[†,‡] Jennie L. Thomas,[§] Daniel D. Kemp,[#] Barbara J. Finlayson-Pitts,[§] Mark S. Gordon,[*,#] Douglas J. Tobias,[*,§] and R. Benny Gerber[*,†,§]

Department of Physical Chemistry and the Fritz Haber Research Center for Molecular Dynamics, Hebrew University, Jerusalem 91904, Israel, Department of Chemistry and AirUCI, University of California, Irvine, California 92697-2025, and Department of Chemistry, Iowa State University, Ames, Iowa 50011

Received: July 24, 2009; Revised Manuscript Received: September 21, 2009

Structural properties of large $NO_3^-\cdot(H_2O)_n$ ($n = 15-500$) clusters are studied by Monte Carlo simulations using effective fragment potentials (EFPs) and by classical molecular dynamics simulations using a polarizable empirical force field. The simulation results are analyzed with a focus on the description of hydrogen bonding and solvation in the clusters. In addition, a comparison between the electronic structure based EFP and the classical force field description of the 32 water cluster system is presented. The EFP simulations, which focused on the cases of $n = 15$ and 32, show an internal, fully solvated structure and a "surface adsorbed" structure for the 32 water cluster at 300 K, with the latter configuration being more probable. The internal solvated structure and the "surface adsorbed" structure differ considerably in their hydrogen bonding coordination numbers. The force field based simulations agree qualitatively with these results, and the local geometry of NO_3^- and solvation at the surface-adsorbed site in the force field simulations are similar to those predicted using EFPs. Differences and similarities between the description of hydrogen bonding of the anion in the two approaches are discussed. Extensive classical force field based simulations at 250 K predict that long time scale stability of "internal" NO_3^-, which is characteristic of extended bulk aqueous interfaces, emerges only for $n > 300$. Ab initio Møller−Plesset perturbation theory is used to test the geometries of selected surface and interior anions for $n = 32$, and the results are compared to the EFP and MD simulations. Qualitatively, all approaches agree that surface structures are preferred over the interior structures for clusters of this size. The relatively large aqueous clusters of NO_3^- studied here are of comparable size to clusters that lead to new particle formation in air. Nitrate ions on the surface of such clusters may have significantly different photochemistry than the internal species. The possible implications of surface-adsorbed nitrate ions for atmospheric chemistry are discussed.

I. Introduction

The nitrate anion (NO_3^-) is one of the most abundant ions in the atmosphere.[1,2] It plays an important role in many atmospheric chemical[1,2] and biological[3,4] processes. The chemistry and the photochemistry of NO_3^- ions in aqueous aerosols may strongly depend on whether the ions are solvated in the bulk or whether they are present at the surface of the aerosol.[5] Therefore, understanding the solvation of NO_3^- and its propensity for the surface of aqueous solutions is important.

The behavior of nitrate ions at the air−solution interface of aqueous nitrate solutions has been the subject of a growing number of experimental investigations in recent years. Nonlinear vibrational spectroscopic measurements that probe environments lacking inversion symmetry, specifically, vibrational sum frequency generation (SFG) and second harmonic generation (SHG), have been used to study the interfaces of aqueous nitrate solutions. SFG spectra covering the range of frequencies of water O−H stretching vibrations have provided indirect evidence for the presence of nitrate ions in the vicinity of the air−water interface signaled by their perturbation of the water hydrogen bonding network.[6,7] The presence of nitrate in the interfacial region has also been demonstrated by direct SFG detection of the nitrate symmetric stretching mode.[8] However, SFG measurements are not capable of determining the precise location and details of the solvation of the ions, nor their relative concentration in the interfacial region versus the bulk. UV-SHG experiments have also been employed to directly probe the presence of nitrate at the air−water interface.[9] The concentration dependence of the SHG intensity could be fit to a Langmuir adsorption isotherm, consistent with nitrate adsorption at the interface, but the free energy of adsorption could not be determined precisely from the fits. Thus, as in the case of the SFG data, the SHG data do not permit the amount of nitrate in the interfacial region to be accurately quantified. Electrospray ionization mass spectrometry measurements suggest that the affinity of nitrate for the air−water interface is slightly greater than that of bromide,[10] an ion that is generally considered to adsorb to the interface.[11] In contrast, analysis of surface tension data based on a thermodynamic partitioning model has led to the conclusion that the concentration of nitrate at the air−water

* To whom correspondence should be addressed. E-mail: mark@si.msg.chem.iastate.edu (M.S.G.), dtobias@uci.edu (D.J.T.), and benny@fh.huji.ac.il (R.B.G.).
† Hebrew University.
‡ Currently at Center for Cancer Research Nanobiology Program, NCI-Frederick, Frederick, MD 21702.
§ University of California.
# Iowa State University.

10.1021/jp9070339 CCC: $40.75
Published on Web 10/09/2009

interface is the same as that in the bulk.[12] Very recently, depth-resolved X-ray photoemission measurements were used to directly measure the concentration profile of nitrate ions at the air−solution interface.[13] These experiments clearly showed that nitrate is present in the interfacial region but at a substantially lower concentration than in the bulk.

The first molecular dynamics (MD) simulation study of the behavior of nitrate at the air−solution interface suggested that nitrate has a propensity to adsorb to the air−water interface.[13,14] This conclusion was reached on the basis of the observation that the nitrate ion remained at the interface for several hundred picoseconds when a polarizable force field was employed. The force field results were corroborated by a density functional theory (DFT) MD simulation of a $NO_3^-\cdot(H_2O)_{10}$ cluster, in which the forces were obtained from the electronic structure computed via DFT with the BLYP exchange-correlation functional, that demonstrated the preference of the ion for the surface of the cluster.[14] Although the cluster results have not yet been called into question, subsequent more extensive force field based studies of nitrate at extended bulk solution−air interfaces have consistently predicted that, while the nitrate ion is capable of visiting the interface, its concentration in the interfacial region is substantially depleted relative to the bulk solution,[15−17] in contrast to the original suggestion of a pronounced interfacial propensity.[13,14] A careful comparison with X-ray photoemission data has demonstrated semiquantitative agreement between the depth-dependence of the nitrate concentration extracted from the experimental data and that predicted by one of the more recent MD simulations employing a polarizable force field.[13]

A full understanding of the role of the interfacial environment in determining the reactivity of nitrate ions at aqueous surfaces in the atmosphere requires a more detailed description of the microsolvation of nitrate in interfacial settings over a range of atmospheric conditions. Electronic structure calculations and spectroscopic measurements have provided insight into the solvation of nitrate in small clusters containing up to six water molecules at low temperatures,[18−22] but data on larger clusters at ambient temperatures is lacking.

We focus here on the solvation of NO_3^- in relatively large water clusters, which are of interest for several reasons. First, while clusters are small compared with bulk systems, they may nevertheless provide insights into the behavior in the condensed phase and at extended bulk interfaces. Second, small to modest-sized clusters can be modeled realistically by more rigorous methods, and such systems can therefore serve as a proving ground for tools used for larger clusters and extended interfacial systems. Finally, the investigation of the dependence of various properties on cluster size may provide new fundamental insights into the bulk versus interfacial solvation of nitrate ions.

One of the main challenges in theoretical investigations of ion solvation is the development of an accurate description of ion−solvent interactions. One can gain insight into ion−water interactions at the molecular level by using a quantum mechanical description of the forces. Molecular anions have complex charge distributions, so that electronic structure-based methods have unique advantages. However, an obvious disadvantage is the prohibitive increase in cost as the cluster size grows. Thus, empirical force fields are presently the most practical tool available for the theoretical investigation of the solvation of anions in very large water clusters and in bulk solution. Comparison of the two approaches for clusters of intermediate sizes is therefore of considerable value for establishing the accuracy of force fields.

In this paper, we report a theoretical study of the solvation of NO_3^- in water clusters, $NO_3^-\cdot(H_2O)_n$, with $n = 32-500$, that employed three approaches. The first is Monte Carlo (MC) simulations based on an electronic structure-based potential called the "effective fragment potential" (EFP). The EFP method is feasible for cluster sizes of up to 32 or more water molecules and can be used to test the empirical force field. The second method is classical MD simulations based on an empirical polarizable force field. The third method is second order Møller−Plesset perturbation theory (MP2), which is used to optimize selected structures for $n = 32$. The empirical force field is computationally applicable to larger clusters and bulk solutions. Thus, we present EFP results for $n = 15$ and $n = 32$, and we use $n = 32$ for detailed comparisons with the force field based simulations and MP2. We also investigate the dependence of the surface propensity of NO_3^- on cluster size using force field based simulations of clusters with $n = 100$, 300, and 500 water molecules. Both the EFP and the force field based simulations predict that NO_3^- strongly prefers to reside on the surface of the cluster with $n = 32$, while MP2 predicts that surface structures are slightly preferred over the interior structures. The force field based simulations predict that the surface propensity persists in clusters as large as $n = 300$, and that the preference of NO_3^- for the interior that has been demonstrated by both simulation and experimental investigations of bulk solutions[13,15−17] does not set in until $n > 300$ water molecules. The implications of the surface preference for NO_3^- in large clusters ($n = 15-300$) for atmospheric chemistry are discussed.

II. Methods

A. Effective Fragment Potential (EFP) Calculations. The EFP method, developed by Gordon and co-workers,[23,24] is a semiclassical model potential, derived from electronic structure theory, for computing intermolecular interactions between solutes and solvents or between solvent molecules. Central to the EFP is the evaluation of the charge distribution within the molecules based on first principles algorithms. The EFP approach has been successfully applied to the solvation of atomic anions in water clusters ($X^-\cdot(H_2O)_n$).[25,26] This paper presents the first application of the EFP approach to a solvated molecular anion, NO_3^-.

Global minimum energy structure searches were performed using the MP2 level of theory and the DH(d,p)[27] basis set for the NO_3^- anion. All of the water molecules were treated within the EFP framework. The general atomic and molecular electronic structure system GAMESS[28] was used for all of the EFP-based calculations.

Searches for the minimum energy structures, including the global minimum on the $NO_3^-\cdot(H_2O)_{32}$ potential energy surfaces, used a MC[29]/simulated annealing (SA)[30] code. The utilization of MC with EFP and the use of EFP itself have several advantages over electronic-structure methods and force field potentials. First, the EFP method can be used directly with MC simulations and thus is applicable to sampling an equilibrium thermodynamic distribution of structures, while with ab initio electronic structure methods, only optimized structures can usually be obtained, because of the limitations of computer resources. For the calculation of room-temperature properties of floppy systems such as ion−water clusters, thermal fluctuations are clearly essential. Second, the energies of the equilibrium structures have been corrected with zero point energies, while in classical MD simulations, quantum effects are not taken into account. Finally, the EFP is not subject to the potential

fitting and parametrization errors that could affect the accuracy of empirical force field based descriptions of NO_3^-/water interactions.

MC/SA was used to initiate structure searches at 600 K and then to slowly cool the systems to 300 K. Geometry optimizations (at 0 K) were performed after every 10 steps in the MC simulations. All of the energies reported here include zero point energy (ZPE) corrections obtained from the Hessian, which is the matrix of the second derivative of the potential energy with respect to the nuclear coordinates. The total number of local minimum structures collected from the simulations for $NO_3^-\cdot(H_2O)_{32}$ is 35. All of the structures that were sampled in the simulations were verified to be local minima by ensuring that no negative eigenvalues (corresponding to imaginary frequencies) were present in the Hessian.

The population, P_j, of each structure j extracted from the simulations is computed using eq 1:

$$P_j = \frac{e^{-\Delta E_j/k_BT}}{\sum_j e^{-\Delta E_j/k_BT}} \quad (1)$$

where ΔE_j is the energy difference between the jth structure and the global minimum structure of a given cluster, $T = 300$ K, and k_B is the Boltzmann constant. Average energies are computed using eq 2:

$$\langle E \rangle = \sum_j P_j E_j \quad (2)$$

in which the sum runs over the structures in a given class (e.g., structures with NO_3^- on the surface or in the interior of the cluster).

B. Polarizable Force Field Based MD Simulations. Simulations of clusters containing one NO_3^- ion and a given number of water molecules ($n = 32$, 100, 300, and 500) were performed using classical molecular dynamics. In order to obtain stable clusters, the velocities were reassigned periodically during the simulation to provide an average temperature of 250 K. For the cluster containing 32 waters, the velocities were reassigned every 100 time steps, while for the larger clusters the velocities were reassigned every 1000 time steps. All simulations were carried out using the Amber 8 suite of programs.[31] The internal degrees of freedom of the water molecules were constrained using the SHAKE algorithm.[32] All of the simulations consisted of 500 ps equilibration followed by 3 ns production runs using a time step of 1 fs. For clusters containing up to 300 waters, all pair interactions were calculated explicitly (i.e., the nonbonded interactions were not truncated). For the 500 water cluster, periodic boundary conditions were employed, and the electrostatic interactions were calculated using the particle mesh Ewald method[33,34] with a neutralizing background and a real space cutoff of 12 Å. The 500 water cluster was placed in a large cubic box with an edge length of 150 Å to approximate an isolated cluster.

A polarizable force field was used for both water and NO_3^-. Water molecules were modeled using the POL3 water model.[35] The force field for nitrate, adapted from the model used by Salvador and co-workers,[14] represents the polarizability by equal contributions from each NO_3^- oxygen ($\alpha = 1.49$ Å^3). The nitrate ion geometry is fixed using artificial O−O bonds in the simulations. The nitrate force field parameters used in the present study are summarized in Table 1. In order to avoid the polarization catastrophe,[36] induced dipoles have been calculated using a method developed previously with the scaling chosen to preserve the properties of neat water.[37] The force field employed here has been shown to perform well at reproducing the thermodynamic properties and composition of bulk interfaces of concentrated nitrate solutions.[13,17]

TABLE 1: Polarizable Force Field Parameters for NO_3^- Used in the Present Study Given in the Amber[31] Convention[a]

atom	q (e)	α (Å^3)	R_{min} (Å)	ϵ (kcal/mol)
N (nitrate)	+0.950	0.000	1.880	0.170
O (nitrate)	−0.650	1.490	1.800	0.160

[a] q is the atomic charge; α is the atomic polarizability, and R_{min} and ϵ are the position and depth of the minimum, respectively, of the Lennard-Jones potential.

C. Møller−Plesset Perturbation Theory (MP2). To examine the structures obtained from EFP simulations, MP2 single point energies were calculated for all 35 of the $n = 32$ structures. Then, three structures were chosen from the EFP simulations at $n = 32$ for further optimization using MP2: the global minimum structure (a surface anion) and the two lowest-energy interior anion structures. All water molecules were represented with MP2, rather than EFP potentials. The DH(d,p) basis set used to describe the anion in the EFP simulations was used for every atom in the MP2 optimizations. For a system of this size, it is not feasible to use larger basis sets. MP2 calculations scale as N^5, where N is the number of basis functions, and each single-point MP2 calculation for the $n = 32$ cluster is, therefore, quite costly. Thus, the MP2 calculation for this large system with the basis set used is a state-of-the-art effort.

III. Results and Discussion

A. Simulations with Effective Fragment Potentials: Structural Properties of $NO_3^-\cdot(H_2O)_{32}$. ***1. Distribution of Structures with NO_3^- in the Interior and on the Surface.*** In this section, we characterize the solvation of NO_3^- both in the interior and on the surface of water clusters using configurations generated with the EFP method. The total number of different structures collected from the simulation of $NO_3^-\cdot(H_2O)_{32}$ is 35. Among these, NO_3^- is in the interior in 6 of the configurations and on the surface in 29 configurations. All of the structures sampled in the simulation are either local minima or the global minimum.

Two surface structures with relatively high population probabilities were predicted using MP2 energies at the EFP geometries. The global minimum, which is statistically the most important structure found in the simulations, predicts that NO_3^- will reside on the surface of the cluster (Figure 1a). The surface structure shown in Figure 1b is nearly isoenergetic with the global minimum, with only ∼0.01 kcal/mol separating them. The populations of the structures are computed using eq 1. These two structures (Figure 1a,b) are fairly similar, and the percentage of population for each of these two structures is 45%; that is, together they represent 90% of the population. Another surface adsorbed structure that constitutes a relatively minor population (1%) is shown in Figure 1c. This surface structure differs from the other two lower energy surface structures primarily with respect to the arrangement of the water molecules. The energy difference between the surface structure shown in Figure 1c and the global minimum surface structure is only ∼1 kcal/mol. The slightly higher energy of the structure in Figure 1c versus the structures in Figure 1a,b is presumably due to the presence of a couple of water molecules with low hydrogen bonding

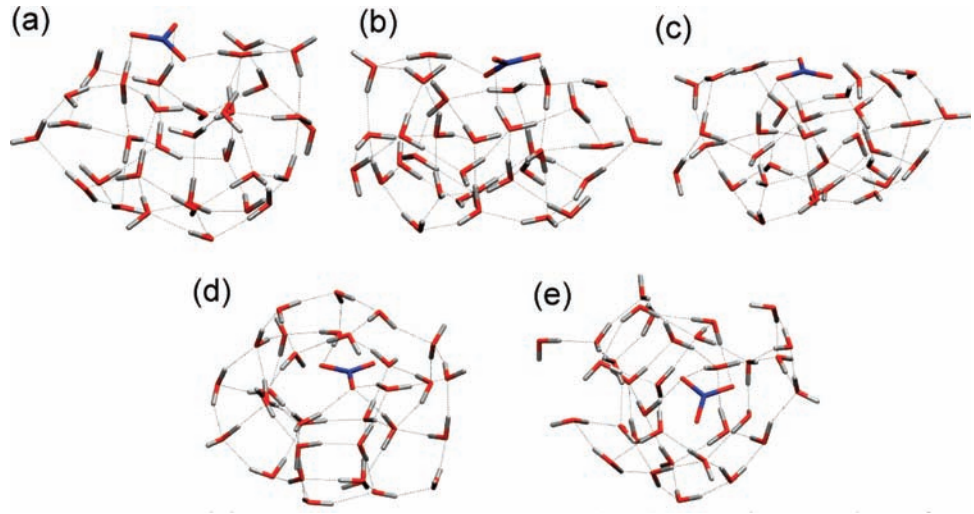

Figure 1. EFP minimum energy structures for $NO_3^-\cdot(H_2O)_{32}$: (a) nitrate on the surface, global minimum structure; (b,c) nitrate on the surface, local minima; (d) nitrate inside the cluster, local minimum; (e) second lowest-energy interior anion structure. Coloring scheme used throughout the paper: O, red; N, blue; H, light gray. Hydrogen bonds, defined by a geometric criterion ($O_{water}\cdots O_{nitrate}$ distance < 3.0 Å, $O_{nitrate}\cdots O_{water}-H_{water}$ angle < 30°), are shown as dotted black lines.

coordination. The population of each of the other 26 surface structures obtained in the simulations (not shown here) is much less than 1%, and the energy differences of these structures from the global minimum are in the range of 3−20 kcal/mol. The sum of the populations of all of these other structures is only ∼8%.

Six interior structures were obtained in the simulations, but there is only one significant interior structure due to its greater stability than the other interior structures. The population of the lowest energy interior structure, shown in Figure 1d, is only $\sim 4 \times 10^{-4}$%. The energy difference between this structure and the global minimum surface structure is 7 kcal/mol. The contribution of each of the other 26 surface structures obtained in the simulations (not shown here) is much less than 1%, and the energy difference of these structures from the global minimum is relatively high. For example, the energy difference between the second-lowest energy interior structure (Figure 1e) relative to the global minimum (Figure 1a) is 12.8 kcal/mol. The population ratio between surface and interior structures is 99.9996:0.0004. Thus, it is safe to say that, in the relatively small $n = 32$ cluster, the NO_3^- is almost always on the surface and almost never inside the cluster at the MP2/EFP level of theory.

The average energies of both the surface and the interior structures of $NO_3^-\cdot(H_2O)_{32}$ were computed using eq 2. The difference between the average energy of the interior structures and the average energy of the surface structures (see eq 2), 7 kcal/mol, is a measure of the stability of the surface versus interior of NO_3^- in a cluster of 32 water molecules at the MP2/EFP level of theory.

2. Structure and Solvation of NO_3^- at the Surface and in the Interior. The structural properties of both surface and interior structures are characterized using the following four properties: the number of solvated O atoms of the NO_3^-, the number of water molecules that have hydrogen bonds with the three O atoms in NO_3^-, the lengths of hydrogen bonds between NO_3^- and water molecules, and the $N_{nitrate}-O_{nitrate}-H_{water}$ (NOH) angle.

We define the number of solvated O atoms as the number of O atoms of NO_3^- that are hydrogen bonded to water molecules. The criterion used to define a hydrogen bond is a distance less than 2 Å. The number of solvated O atoms in NO_3^- for the surface structures of $NO_3^-\cdot(H_2O)_{32}$ is predominately one (∼43%) or two (∼47%). Only a few structures (∼10%) have all three oxygen atoms in NO_3^- hydrogen bonded to water molecules. In a few cases, one O atom in NO_3^- has more than one hydrogen bond. For the interior structures, the number of solvated O atoms in NO_3^- is either two (∼55%) or three (∼45%).

The coordination number is defined as the number of water molecules that hydrogen bond with the O atoms in NO_3^-. There may be more than one water molecule that participates in hydrogen bonding with an individual O atom in NO_3^-. The coordination numbers predicted for the surface structures of $NO_3^-\cdot(H_2O)_{32}$ are in the range of 1−4, with the most probable number of water molecules around the ion being 2 or 3. For interior structures, the coordination numbers are predominantly 3 and 4 (86% of the structures), and 5 in relatively few cases (14% of the structures). As expected, the coordination numbers for the interior structures are larger than those for the surface structure.

Additional information on the solvation of nitrate in $NO_3^-\cdot(H_2O)_{32}$ is provided by the distribution of the distances between each of the nitrate O atoms and the H atoms of coordinating water molecules. It is found that 48% of the structures with nitrate on the surface have $O_{nitrate}-H_{water}$ distances of 1.95−2.00 Å, 36% have distances of 1.90−1.95 Å, and only 16% have distances of 1.85−1.90 Å. In the interior structures, the most probable value of the hydrogen bond distance is in the range 1.85−1.90 Å. Thus, the distribution is shifted to shorter distances, and this indicates that the NO_3^-/water hydrogen bonding is stronger for the interior structures. The fact that the interior site is much higher in total energy than the surface is most likely due to the disruption of the water−water hydrogen-bonded network in the interior sites. Thus, while NO_3^- can make reasonably strong hydrogen bonds with water molecules, these do not sufficiently compensate for the disruption of water−water hydrogen bonds, at least in small clusters.

The $N_{nitrate}-O_{nitrate}-H_{water}$ (NOH) angle provides a metric for discriminating between interior and surface solvation of NO_3^-. The preferred angle for both interior and surface structures lies in the range 90−110°; 38% of the interior structures have an angle of 90−100°, while 46% of the surface structures have an angle of 100−110°. The interior structures have a small

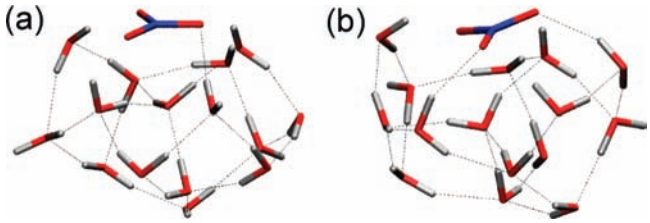

Figure 2. EFP minimum energy structures for $NO_3^-\cdot(H_2O)_{15}$: (a) nitrate on the surface, global minimum; (b) nitrate on the surface, local minimum. Dotted black lines indicate hydrogen bonds defined using the geometric criterion given in the caption to Figure 1.

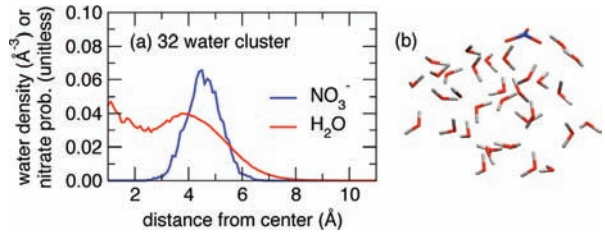

Figure 3. (a) Water density profile (red curve) and radial probability distribution of the nitrate N atom (blue curve) plotted vs the distance from the center-of-mass in the force field based MD simulation of $NO_3^-\cdot(H_2O)_{32}$. (b) Snapshot from the MD simulation of $NO_3^-\cdot(H_2O)_{32}$.

population (∼4%) of angles in the range of 140−150°, while none of the surface structures have NOH angles in this range.

B. Cluster Size Effect in the Small Cluster Regime: $NO_3^-\cdot(H_2O)_{15}$ versus $NO_3^-\cdot(H_2O)_{32}$. In contrast to $n = 32$, for which there is a stable local minimum with the nitrate ion in the interior of the cluster (albeit with very low population), there is (on the basis of the EFP calculations) no stable interior site for $n = 15$. There are, however, several distinct surface structures. The global minimum, which is statistically the most important structure found in the simulations (58% population), is the surface adsorbed structure shown in Figure 2a. The surface structure that is depicted in Figure 2b is a local minimum with a population of 38%, which is ∼0.25 kcal/mol higher in energy than the global minimum structure. The populations of the other surface structures obtained in the simulations (not shown here) are 1% or smaller, and the energy differences of these structures from the global minimum are in the range of 2−10 kcal/mol.

The number of solvated nitrate O atoms for the $NO_3^-\cdot(H_2O)_{15}$ surface structures is predominately one or three (33% for one solvated O atom and 33% for three solvated O atoms). However, 18% of the structures have two nitrate O atoms hydrogen bonded to water molecules. As noted earlier, the number of solvated nitrate O atoms in $NO_3^-\cdot(H_2O)_{32}$ surface structures is predominately one or two. Only a few structures (∼10%) have three NO_3^- oxygen atoms that are hydrogen bonded to water molecules.

The coordination numbers predicted for the $NO_3^-\cdot(H_2O)_{15}$ surface structures are in the range of 1−3, with the most probable number of water molecules around the ion being 1−2 (∼84% of the population). This can be compared to the coordination numbers predicted for the surface structures of $NO_3^-\cdot(H_2O)_{32}$, which are in the range of 1−4, with the most probable number of water molecules around the ion being 2−3.

For the $NO_3^-\cdot(H_2O)_{15}$ surface structures, 45% have hydrogen bond distances of 1.95−2.00 Å, 37% have hydrogen bond distances of 1.90−1.95 Å, 16% have hydrogen bond distances of 1.85−1.90 Å, and only 2% have hydrogen bond distances of 1.80−1.85 Å. This is very similar to that found for the cluster with 32 water molecules, indicating that the hydrogen bond distances are not very sensitive to cluster size.

The preferred NOH angle for $NO_3^-\cdot(H_2O)_{32}$ surface structures lies between 90−110°, as 48% of the surface structures have an angle of 100−110°. For the smaller $NO_3^-\cdot(H_2O)_{15}$ cluster, the preferred angle in surface structures also lies in the range 90−110°; 31% of the surface structures have an angle of 100−110°. However, 24% of the surface structures of $NO_3^-\cdot(H_2O)_{15}$ have angles lying between 120 and 130°.

To summarize the results of the EFP calculations reported thus far, the $n = 15$ and $n = 32$ clusters differ somewhat in their structural properties, insofar as the location of the NO_3^- ion is concerned. The $n = 15$ cluster has more than one important surface-like structure. This cluster may be more "floppy" and structureless because it is very small. However, for $n = 32$, both well-defined surface and internal structures are predicted, although the surface location is overwhelmingly more favorable energetically, and one can describe the solvating water molecules as forming a "droplet" shape.

C. Structure and Ion Solvation in $NO_3^-\cdot(H_2O)_{32}$: Force Field Based MD Simulations Versus EFP. The relatively minor computational cost of the empirical force field permits extensive sampling of the ion position and solvation in large nitrate−water clusters during a MD simulation at 250 K. The MD simulation of $NO_3^-\cdot(H_2O)_{32}$ was initiated with the ion in the center of the cluster. The ion rapidly went to the surface of the cluster during the equilibration and never returned to the interior during the 3 ns production run. The water O radial density profile, $\rho(r)$, and the probability of finding the nitrate N atom at a distance r from the cluster center-of-mass are plotted in Figure 3a. The water density is consistent with a diffuse droplet shape with an average radius of ∼5 Å. The NO_3^- probability distribution shows that the ion is exclusively located on the surface of the cluster, on average, ∼4.5 Å from the center-of-mass. The representative snapshot from the MD simulation depicted in Figure 3b shows that cluster shape and the ion arrangement on the cluster are similar to the corresponding attributes of the highest probability clusters generated by the EFP (Figure 1a−c). Thus, both the force field and the EFP predict that the predominant structures of $NO_3^-\cdot(H_2O)_{32}$ have the nitrate ion sitting on the surface with its plane parallel to the water−vacuum "interface".

Although the force field and EFP agree that NO_3^- predominantly resides on the surface of $NO_3^-\cdot(H_2O)_{32}$, there are some noteworthy discrepancies in the details of the ion solvation predicted by the two methods. For example, the $O_{nitrate}-H_{water}$ radial distribution functions $g(r)$ plotted in Figure 4 reveal subtle differences in hydrogen bonding. The EFP result was computed by only considering configurations in which the NO_3^- ion is on the surface of the cluster. While the $g(r)$ computed from the EFP-generated configurations is noisier because of limited sampling, both the EFP and the force field results display sharp first and relatively broad second peaks, indicating the existence of a tight first and diffuse second solvation shell. The positions of the first and second peaks from the force field based simulation, 1.8 Å and 3.1 Å, respectively, are significantly smaller than the corresponding values from the EFP calculations, 2.1 Å and 3.4 Å, respectively. Thus, the force field predicts shorter nitrate−water hydrogen bonds than the EFP.

Additional details on the nitrate−water interactions are provided by the histograms of the number of nitrate O atoms that are solvated by water molecules, plotted in Figure 5 as a function of the $O_{nitrate}-H_{water}$ cutoff distance used to define a nitrate−water hydrogen bond. Overall, these plots are consistent with the conclusion from the $g(r)$ data that the force field predicts

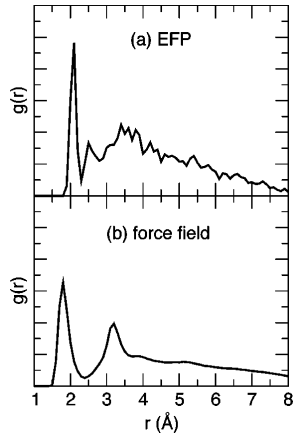

Figure 4. Radial distribution functions of water H atoms around nitrate O atoms in $NO_3^-\cdot(H_2O)_{32}$ clusters computed from (a) minimum energy configurations from EFP calculations with the nitrate ion on the surface of the cluster and (b) configurations from the force field based MD simulation. Because of the lack of a well-defined reference density to normalize $g(r)$ for these small cluster systems, the absolute scale is arbitrary and has therefore been omitted.

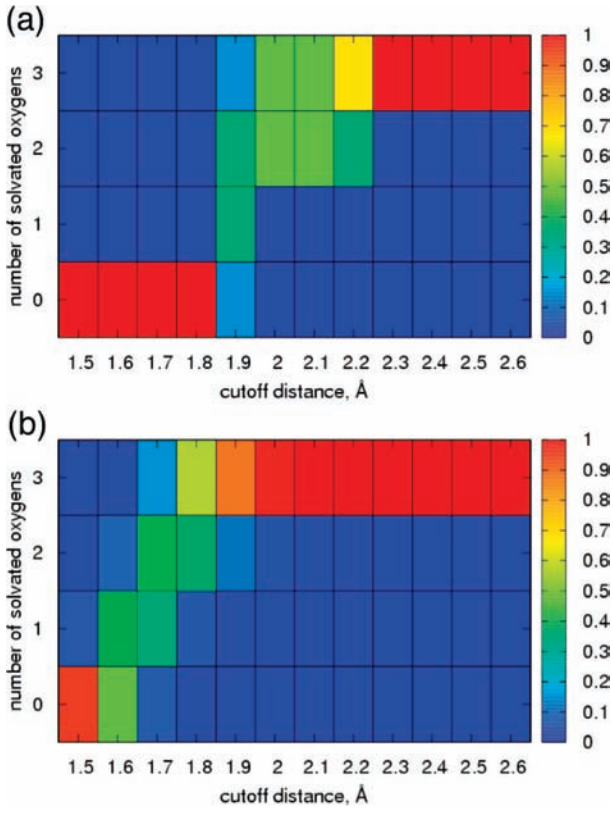

Figure 5. Probability of observing a specific number of solvated nitrate oxygen atoms as a function of the $O_{nitrate}-H_{water}$ hydrogen bonding cutoff distance in $NO_3^-\cdot(H_2O)_{32}$ clusters. (a) Minimum energy configurations from EFP calculations with the nitrate ion on the surface of the cluster. (b) Configurations from the force field based MD simulation.

shorter hydrogen bonds than the EFP method does, in the sense that more hydrogen bonds are counted at short cutoff distances in the force field results versus the EFP. In the discussion of liquid structure, the position of the first minimum in $g(r)$ is used to define the spatial extent of the first solvation shell. If the hydrogen bond cutoff is defined by the position of the first minimum in the $O_{nitrate}-H_{water}$ $g(r)$, which occurs at 2.3−2.4 Å, then both the EFP and the force field based simulations

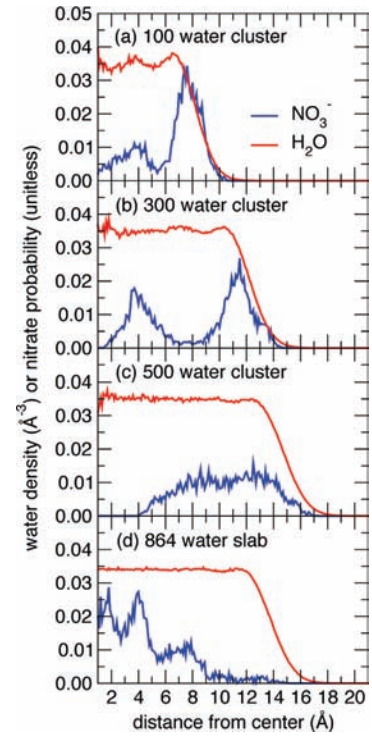

Figure 6. Water density profiles (red curves) and probability distributions of the nitrate N atom (blue curves) plotted vs the distance from the center-of-mass in the force field based MD simulations of (a) $NO_3^-\cdot(H_2O)_{100}$ cluster, (b) $NO_3^-\cdot(H_2O)_{300}$ cluster, (c) $NO_3^-\cdot(H_2O)_{500}$ cluster, and (d) 864 water slab (bulk).

consistently predict that all three nitrate O atoms are solvated essentially all of the time when the ion is on the surface of the cluster.

Overall, the preferred nitrate ion location and solvation in $NO_3^-\cdot(H_2O)_{32}$ predicted by the empirical polarizable force field used in this work compares favorably with the more accurate, but computationally costly, electronic structure-based EFP method. In addition to validating the qualitative predictions of the force field, the fact that a consistent picture emerges from both approaches testifies to the robustness of the results.

D. Classical Polarizable Force Field Simulations of $NO_3^-\cdot(H_2O)_n$, $n = 100$, 300, and 500: Evolution of Structural Properties with Cluster Size. The strong surface propensity of nitrate in modest-sized (15−32 water) clusters is qualitatively different from the behavior of nitrate near extended interfaces of bulk aqueous solutions. The consensus that has emerged recently from both theoretical and experimental studies is that nitrate approaches the air−solution interface but does not strongly adsorb in concentrated bulk solutions.[9,13−17] It is therefore expected that a crossover in the preference from surface to interior solvation should be observed in clusters at some point as the cluster size is increased. We have investigated the cluster size-dependence of nitrate solvation by performing additional empirical force field based simulations of nitrate−water clusters with $n = 100$, 300, and 500 water molecules.

Water radial density profiles that define the extent of the cluster are plotted in Figure 6 along with the probability of finding the nitrate N atom at a distance r from the center-of-mass of clusters with $n = 100$, 300, and 500 water molecules. For comparison, the water density profile and nitrate distribution obtained from a simulation of a single nitrate ion in a slab of 864 water molecules with periodic boundary conditions that generate an extended bulk air−water interface are shown in

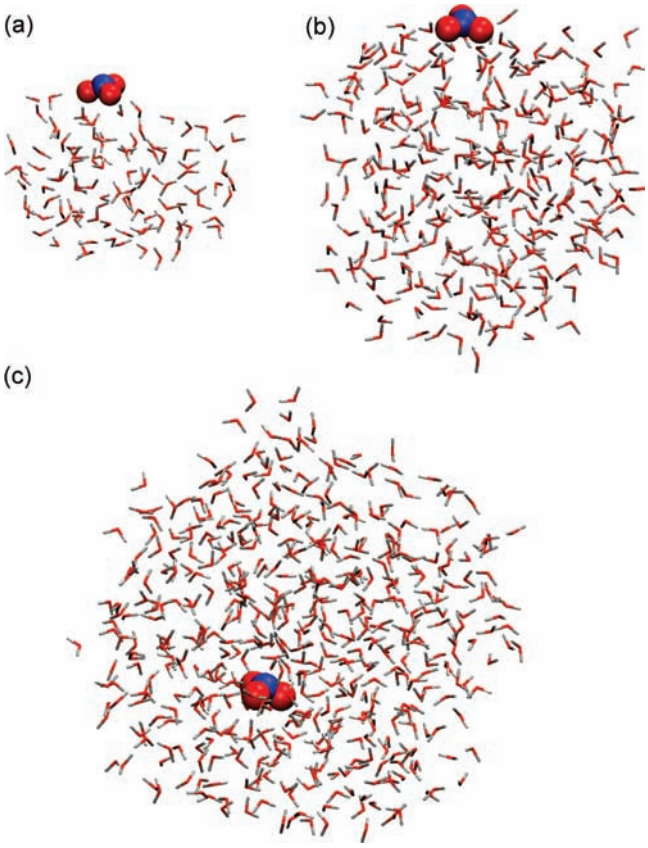

Figure 7. Representative snapshots from the force field based MD simulations of (a) $NO_3^-\cdot(H_2O)_{100}$, (b) $NO_3^-\cdot(H_2O)_{300}$, and (c) $NO_3^-\cdot(H_2O)_{500}$. The snapshots depict the preferred surface location of nitrate in the 100 and 300 water clusters and the preferred interior location in the 500 water cluster.

Figure 6d. The data plotted in Figure 6d confirm that the nitrate ion prefers the interior and avoids the surface of the solution in an extended interfacial setting. In the 100 and 300 water clusters, the nitrate probability distribution displays two peaks, corresponding to interior and surface locations of the ion. In the 100 water cluster, the population at the surface is about three times greater than the interior, while in the 300 water cluster, the surface is only slightly favored over the interior. In the 500 water cluster, a distinct surface population is no longer discernible, and population of nitrate that is well-solvated in the interior of the cluster clearly exceeds that near the surface of the cluster. Snapshots depicting the preferred location of nitrate in clusters with $n = 100$, 300, and 500 water molecules are shown in Figure 7.

In summary, this study shows that the nitrate anion in water clusters prefers to lie on the surface of the smaller clusters considered here ($n = 15$, 32, 100, and 300 water molecules). However, this preference decreases with an increase in the cluster size. For a relatively large cluster consisting of 500 water molecules, the nitrate anion no longer displays strong surface adsorption, and it spends the majority of the time well-solvated in the interior of the cluster. This decrease in surface propensity is presumably driven, in part, by entropy because of an increase in the ratio of interior sites to surface sites as the size of the cluster increases. There could also be an energetic component associated with the organization of the solvent shells around the ion.

Analysis of nitrate solvation using MD simulations of bulk solutions reveals a diffuse solvent shell around nitrate, which is manifested as a broad split first peak in the $N_{nitrate}-O_{water}$ radial distribution function, that contains ~18 water molecules and extends to ~5 Å from the N atom.[17] A reasonable hypothesis is that the interior location of the nitrate ion is disfavored in the smaller clusters because of the inability to support the complex solvent organization around the ion that is preferred in bulk solution. This hypothesis is supported by the $O_{nitrate}-O_{water}$ radial distribution functions plotted in Figure 8, which display two prominent peaks. Except for a disparity in scale due to the difference in the normalization of bulk and cluster radial distribution functions, the $g(r)$ for nitrate on the interior of the 500 water cluster is essentially identical to that of nitrate in the interior of the extended slab. Thus, the interior of the 500 water cluster supports the solvation environment preferred by nitrate in dilute bulk solution. In contrast, the second peak in the $g(r)$ for nitrate on the interior of the 300 water cluster is suppressed, indicating, remarkably, that the complex solvation environment preferred by nitrate in bulk solution cannot be fully accommodated in this large cluster. Evidently, the full development of the solvent shells provides additional energetic stabilization that favors the bulk environment in the 500 water cluster and extended slab.

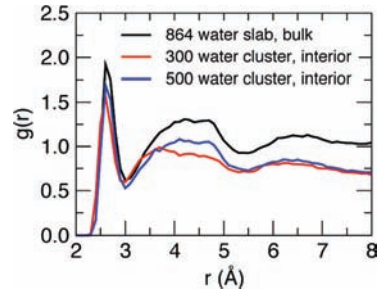

Figure 8. Radial distribution functions of water O atoms around nitrate O atoms from force field based MD simulation configurations in which the nitrate ion is in the interior of clusters or a bulk water slab: red, $NO_3^-\cdot(H_2O)_{300}$; blue, $NO_3^-\cdot(H_2O)_{500}$; black, 864 water slab.

E. Optimization of Surface and Interior Structures by the MP2 Level of Theory. MP2 single point energies were computed for all $n = 32$ structures obtained from MP2/EFP simulations, and the energy differences between the structures were computed as well. To assess the accuracy of the predicted structures obtained from the MP2/EFP simulations, we optimized the structures with the MP2 level of theory, computed the energy differences between the structures, and compared the results to the MP2/EFP level of theory. Since optimization with the MP2 level of theory including the Hessian calculations is computationally expensive, optimization without Hessian calculations were performed for only three selected structures obtained from the MP2/EFP simulations: the global minimum (Figure 1a) and the two lowest-energy interior anion structures (shown in Figure 1d,e). For the $NO_3^-\cdot(H_2O)_{32}$ cluster, both MP2/EFP and MP2 predict that the nitrate prefers to "sit" on the surface rather than be in a bulk solvated environmental. Further, MP2/EFP predicts that the population probabilities of the surface structures are much higher than that of the population probabilities of the interior structures, which are so small that they can be neglected.

However, quantitatively, there are substantial differences between the prediction of the MP2/EFP method and that of the MP2 method in the relative energies between the structures. Table 2 summarizes the differences in the relative energies for the structures shown in Figure 1. For example, while in the MP2/EFP simulations, the energy difference between the surface structure (global minimum; Figure 1a) and the most stable interior structure (Figure 1d) is 6.9 kcal/mol; after MP2

TABLE 2: Comparison of the Relative Energies of Surface and Interior Structures for $NO_3^-\cdot(H_2O)_{32}$ and of the Averaged Hydrogen Bonding Distances for MP2/EFP1 Method and MP2 Level of Theory

structure	MP2/EFP1 relative energy (kcal/mol)	MP2 single point relative energy (kcal/mol)	MP2 optimized relative energy (kcal/mol)	MP2/EFP1 averaged $O_{nitrate}-H_{water}$ distance (Å)	MP2 averaged $O_{nitrate}-H_{water}$ distance (Å)	MP2/EFP1 averaged hydrogen bonding[a] (Å)	MP2 averaged hydrogen bonding[a] (Å)	figure
surface structure	0	2.5	0	1.99	1.91	1.74	1.83	1a
surface structure	0.01	2.5						1b
surface structure	1.0	2.8						1c
interior structure	6.9	0.0	0.5	1.86	1.83	1.78	2.21	1d
interior structure	12.8	8.3	6.9	2.03	1.83	1.74	1.84	1e

[a] Hydrogen bonding between water molecules that are connected to the nitrate ion and other water molecules.

optimization, the energy difference between these two structures is only 0.5 kcal/mol. These results suggest that even though the global minimum structure is a surface anion, interior anion structures may be nearly isoenergetic with the global minimum. Contrary to the results of many studies utilizing inexpensive empirical potentials, it is possible that $n = 32$ is approaching a sufficiently large enough cluster to complete the first solvation shell around the nitrate anion and form an interior anion. This suggests that the hydrogen bonding environment of aqueous nitrate solutions may be too complex to quantitatively study with inexpensive model potentials. Though the quantitative agreement with MP2 is not as good as one would like, it is important to point out that the MP2/EFP simulations did find energetically relevant interior anions. The relatively inexpensive MP2/EFP level of theory is able to obtain energetically relevant minima at much smaller computational cost compared with MP2 calculations. When the structures are obtained with MP2/EFP and the relative energies are calculated with MP2, the most accurate relative energies available for systems of this size can be obtained for a broad sample of structures.

Comparison of the averaged hydrogen bond distances of each of the three selected structures obtained in MP2/EFP simulations and their optimized structures by the MP2 level of theory is summarized in Table 2. The average $O_{nitrate}-H_{water}$ distance differs between the two methods by only 0.08 Å for the lowest energy surface anion (Figure 1a), while the average hydrogen bond distance differs by 0.9 Å. The average hydrogen bonding distances of the interior structures shown in Figure 1d,e differ between the two methods by 0.43 Å and 0.1 Å, respectively. Visual inspection of the structures reveals that the internal geometries of the water molecules change more than the placement of the solvent molecules with respect to the whole cluster. Despite the structural changes that occur during optimization, the relative energies of the optimized structures do not differ much from the MP2 single points.

The quantitative differences between the relative energies at the MP2/EFP and the relative energies at the MP2 level of theory may be due to dispersion. EFP does not include dispersion effects while MP2 does. The charge distribution of the nitrate anion may be complex enough that the dispersion forces between the solute and the solvent molecules may play a key role in determining whether or not the anion is completely solvated. A general potential model, called EFP2, has been developed and includes dispersion. However, it has not yet been fully interfaced with ab initio calculations. Studying the importance of dispersion will be the focus of a future study when the EFP2/ab initio interface is complete.

These results show that solely relying on model potentials may not always provide accurate quantitative results for every cluster size, and checking the results with ab initio methods is necessary. This serves as a reminder of the importance of ab initio calculations and verifying results with the highest level of theory that is computationally feasible.

IV. Atmospheric Relevance of Nitrate−Water Clusters

The formation and growth of new particles in air is important for understanding and predicting their effects on visibility, health, and climate.[38−40] Elucidating the species involved in nucleation in particular has been difficult because of the small size of the clusters and the lack of analytical methods to probe such small amounts of material. While it is clear that sulfuric acid is often responsible for new particle formation, there are intriguing hints that nitrogen may also play a role. For example, nitrogen and organics have often both been found in sub-10 nm sized particles in some studies, with the organic being more closely associated with nitrogen than with sulfate.[41,42] The form of nitrogen in the particles is not well-known but appears to be at least in part, nitrate ions.

The photochemistry of nitrate ions in bulk solution is well-known:[43−45]

$$NO_3^- + h\nu \rightarrow NO_2 + O^- \xrightarrow{H_2O} NO_2 + OH + OH^- \quad (3)$$

$$\rightarrow NO_2^- + O(^3P) \quad (4)$$

The overall quantum yields for production of OH and $O(^3P)$ in bulk solutions are $\phi_3 = 0.009$ and $\phi_4 = 0.001$, respectively, at 305 nm.[43−45] This photochemistry is important under some conditions in the atmosphere, since nitrate is a ubiquitous component of atmospheric aerosols, snowpacks, and urban surfaces.[1] For example, photochemical production of NO_x in snowpacks has been attributed primarily to reactions 3 and 4.[46−53]

There is reason to believe that the photochemistry of nitrate ions may be quantitatively and, perhaps, qualitatively different when the nitrate ion is on the surface compared with the bulk. At the interface, there is an incomplete solvent cage so that one would expect less recombination of NO_2 with O^- and of NO with $O(^3P)$, leading to larger overall quantum yields.[54] A particularly intriguing result from the present study is the high percentage of surface structures that have only one O atom in NO_3^- that is solvated compared with the bulk, where either two or all three O atoms are solvated. In addition, a large percentage of the surface nitrate ions have only one or two water molecules that are hydrogen bonded to O atoms in the nitrate, whereas none in the bulk are so under-coordinated. This significant difference in the interaction of nitrate ions with surrounding water molecules may change the overall quantum yields for OH and $O(^3P)$ production, and potentially also the relative importance of these two pathways. For example, enhanced production of gas phase NO_2 seems likely if the nitrate photolyzes while only one of the oxygen atoms is hydrogen-bonded to water,

compared with the situation in the bulk where two or three of the nitrate oxygen atoms are hydrogen-bonded.

Enhanced production of the oxidants OH and $O(^3P)$ at the interface may result in unique and, as yet, unrecognized photochemistry in the atmosphere. For example, some atmospherically important organic gases such as α-pinene[55] and napthalene[16,56−58] have significant residence times on aqueous surfaces. If there is generation of highly reactive OH and $O(^3P)$ nitrate at the interface by nitrate ion photolysis, then there is the potential for oxidation of the organics adsorbed at the surface. If the volatility of the organic oxidation products is small and/or they are soluble, they will remain associated with the particle. This new mechanism of formation of organics in particles would lead to an association between nitrate and organics, especially in the smallest particles where nitrate is predicted from the current work to reside at the interface. Clusters of 32−300, where the nitrate ion prefers the surface, correspond to particles with diameters of the order of 1−2.5 nm in the atmosphere, where nucleation and growth is in the early stages. Such a mechanism may contribute to the finding of nitrogen and organics in the smallest particles observed in Mexico City by Smith and co-workers.[41,42] In addition, the possibility should be considered that, when nitrate begins to favor the interior for larger clusters, oxidants will continue to be generated at the surface via formation in the bulk followed by diffusion to the interface.

Finally, thin films of water exist on surfaces in the tropospheric boundary layer.[59] Gaseous nitric acid undergoes rapid deposition on such surfaces[1] and is formed on them via heterogeneous chemistry such as the hydrolysis of adsorbed NO_2/N_2O_4.[60] Nitrate is also taken up on urban surfaces by the deposition of nitrate-containing particles. Such surfaces are known to adsorb organics from air.[61−63] Depending on the nature of water on these surfaces, which is currently not well-understood,[64] nitrate ions may prefer the interface in these thin films as well, leading to enhancement of the photochemical oxidations of coadsorbed organics. Relevant to this possibility is recent work on films of organics and nitric acid by Handely et al.[65] in which photochemical loss of HNO_3 was observed and attributed to photoreduction of the HNO_3. Such chemistry on urban surfaces is not currently included in urban airshed models because of the lack of data on such processes but is clearly an area that is potentially important for accurate modeling of urban airsheds and application to development of effective control strategies.

V. Concluding Remarks

The structural properties of nitrate−water clusters, $NO_3^-\cdot(H_2O)_n$, were explored for a large range of cluster sizes, from $n = 15$ to nanodroplets containing several hundred water molecules. For the smallest cluster sizes considered, with $n = 15$ and $n = 32$, the electronic structure-based effective fragment potential (EFP) method was used to compute the structural properties. The fact that the predictions of this method are in good qualitative agreement with polarizable force field based MD simulations lends strong support to the main conclusion of this study, namely, that the nitrate ions have a strong preference for the surface in relatively small water clusters. Even though relatively low-energy interior anions are predicted, MP2 optimizations confirm that the lowest energy structure for $n = 32$ is likely to be a surface anion. This surface preference for small clusters persists, albeit more weakly, for clusters containing hundreds of water molecules with sizes on the order of nanometers. A crossover from a preference for surface solvation to the predominance of interior solvation that is characteristic of bulk solution interfaces is observed to occur between $n = 300$ and $n = 500$ water molecules, although the fully optimized MP2 results suggest that the crossover may occur at smaller cluster sizes. The photochemistry of nitrate anions could be significantly altered by their presence at the surfaces of such water clusters, films, and other systems compared with the bulk, and this may play a role in new particle formation in the atmosphere as well as in the chemistry and photochemistry of nitrate in thin water films on surfaces. Experimental and additional theoretical studies are underway to explore this possibility.

Acknowledgment. R.B.G., B.J.F.P., and D.J.T. acknowledge the support of the AirUCI Environmental Molecular Science Institute (Grant CHE-0431312) funded by the National Science Foundation. B.J.F.P. is also grateful to the U.S. Department of Energy (Grant DE-FG02-05ER64000) for partial support of this work. D.D.K. and M.S.G. acknowledge the support of the Department of Energy Chemical Physics program at the Ames Laboratory, administered by Iowa State University.

References and Notes

(1) Finlayson-Pitts, B. J.; Pitts, J. N. *Chemistry of the Upper and the Lower Atmosphere*; Academic: San Diego, 2000.
(2) Wayne, R. P. *Chemistry of Atmospheres*; Oxford University Press: Oxford, 2000.
(3) Frank, H. *Chemical Physics of Ionic Solutions*; John Wiley and Sons: New York, 1956.
(4) Williams, R. J. P. *Bio-inorganic Chemistry*; American Chemical Society: Washington, DC, 1971.
(5) Nissenson, P.; Knox, C. J. H.; Finlayson-Pitts, B. J.; Phillips, L. F.; Dabdub, D. *Phys. Chem. Chem. Phys.* **2006**, *8*, 4700.
(6) Schnitzer, C.; Baldelli, S.; Shultz, M. J. *J. Phys. Chem. B* **2000**, 585.
(7) Xu, M.; Spinney, R.; Allen, H. C. *J. Phys. Chem. B* **2009**, *113*, 4102.
(8) Xu, M.; Tang, C. Y.; Jubb, A. M.; Chen, X.; Allen, H. C. *J. Phys. Chem. C* **2009**, *113*, 2082.
(9) Otten, D. E.; Petersen, P. B.; Saykally, R. J. *Chem. Phys. Lett.* **2007**, *449*, 261.
(10) Cheng, J.; Vecitis, C. D.; Hoffmann, M. R.; Colussi, A. J. *J. Phys. Chem. B* **2006**, *110*, 25598.
(11) Jungwirth, P.; Tobias, D. J. *Chem. Rev.* **2006**, *106*, 1259.
(12) Pegram, L. M.; Record, M. T., Jr. *Proc. Natl. Acad. Sci. U.S.A.* **2006**, *103*, 14278.
(13) Brown, M. A.; Winter, B.; Faubel, M.; Hemminger, J. C. *J. Am. Chem. Soc.* **2009**, *131*, 8354.
(14) Salvador, P.; Curtis, J. E.; Tobias, D. J.; Jungwirth, P. *Phys. Chem. Chem. Phys.* **2003**, *5*, 3752.
(15) Dang, L. X.; Chang, T. M.; Roeselova, M.; Garrett, B. C.; Tobias, D. J. *J. Chem. Phys*. 2006, *124*.
(16) Minofar, B.; Vacha, R.; Wahab, A.; Mahiuddin, S.; Kunz, W.; Jungwirth, P. *J. Phys. Chem. B* **2006**, *110*, 15939.
(17) Thomas, J. L.; Roeselova, M.; Dang, L. X.; Tobias, D. J. *J. Phys. Chem. A* **2007**, *111*, 3091.
(18) Waterland, M. R.; Stockwell, D.; Kelley, A. M. *J. Chem. Phys.* **2001**, *114*, 6249.
(19) Shen, M. Z.; Xie, Y. M.; Schaefer, H. F.; Deakyne, C. A. *J. Chem. Phys.* **1990**, *93*, 3379.
(20) Howell, J. M.; Sapse, A. M.; Singman, E.; Synder, G. *J. Phys. Chem.* **1982**, *86*, 2345.
(21) Wang, X. B.; Yang, X.; Wang, L. S.; Nicholas, J. B. *J. Chem. Phys.* **2002**, *116*, 561.
(22) Goebbert, D. J.; Garand, E.; Wende, T.; Bergmann, R.; Meijer, G.; Asmis, K. R.; Neumark, D. M. *J. Phys. Chem. A* **2009**, *113*, 7584.
(23) Day, P. N.; Jensen, J. H.; Gordon, M. S.; Webb, S. P.; Stevens, W. J.; Krauss, M.; Garmer, D.; Basch, H.; Cohen, D. *J. Chem. Phys.* **1996**, *105*, 1968.
(24) Gordon, M. S.; Freitag, M. A.; Bandyopadhyay, P.; Jensen, J. H.; Kairys, V.; Stevens, W. J. *J. Phys. Chem. A* **2001**, *105*, 293.
(25) Merrill, G. N.; Webb, S. P. *J. Phys. Chem. A* **2003**, *107*, 7852.
(26) Kemp, D. D.; Gordon, M. S. *J. Phys. Chem. A* **2005**, *109*, 7688.
(27) Dunning, J., T. H. ; Hay, P. J. *Methods of Electronic Structure Theory*; Plenum Press: New York, 1977.

(28) Schmidt, M. W.; Baldridge, K. K.; Boatz, J. A.; Elbert, S. T.; Gordon, M. S.; Jensen, J. H.; Koseki, S.; Matsunaga, N.; Nguyen, K. A.; Su, S. J.; Windus, T. L.; Dupuis, M.; Montgomery, J. A. *J. Comput. Chem.* **1993**, *14*, 1347.

(29) Metropolis, N.; Rosenbluth, A. W.; Rosenbluth, M. N.; Teller, A. H.; Teller, E. *J. Chem. Phys.* **1953**, *21*, 1087.

(30) Kirkpatrick, S.; Gelatt, C. D.; Vecchi, M. P. *Science* **1983**, *220*, 671.

(31) Case, D. A.; Darden, T. A.; Cheatham, T. E., III.; Simmerling, C. L.; Wang, J.; Duke, R. E.; Luo, R.; Merz, K. M.; Wang, B.; Pearlman, D. A.; Crowley, M.; Brozell, S.; Tsui, V.; Gohlke, H.; Mongan, J.; Hornak, V.; Cui, G.; Beroza, P.; Schafmeister, C.; Caldwell, J. W.; Ross, W. S.; Kollman, P. A. *AMBER 8 University of California*, San Francisco, 2004.

(32) Ryckaert, J. P.; Ciccotti, G.; Berendsen, H. J. C. *J. Comput. Phys.* **1977**, *23*, 327.

(33) Darden, T.; York, D.; Pedersen, L. *J. Chem. Phys.* **1993**, *98*, 10089.

(34) Essmann, U.; Perera, L.; Berkowitz, M. L.; Darden, T.; Lee, H.; Pedersen, L. G. *J. Chem. Phys.* **1995**, *103*, 8577.

(35) Caldwell, J. W.; Kollman, P. A. *J. Phys. Chem.* **1995**, *99*, 6208.

(36) Thole, B. T. *Chem. Phys.* **1981**, *59*, 341.

(37) Petersen, P. B.; Saykally, R. J.; Mucha, M.; Jungwirth, P. *J. Phys. Chem. B* **2005**, *109*, 10915.

(38) Kulmala, M.; Vehkamaki, H.; Petaja, T.; Dal Maso, M.; Lauri, A.; Kerminen, V. M.; Birmili, W.; McMurry, P. H. *J. Aerosol Sci.* **2004**, *35*, 143.

(39) Ghan, S. J.; Schwartz, S. E. *Bull. Am. Meteor. Soc.* **2007**, *88*, 1059.

(40) *Climate Change 2007: The Physical Science Basis. IPCC Secretariat*; Geneva, 2007.

(41) Smith, J. N.; Dunn, M. J.; Van Reken, T. M.; Iida, K.; Stolzenburg, M. R.; McCurdy, P. H.; Huey, L. G. *Geophys. Res. Lett.*, submitted 2007.

(42) Smith, J. N.; Moore, K. F.; MuCurdy, P. H.; Eisele, F. L. *Aerosol Sci. Technol.* **2004**, *38*, 100.

(43) Mack, J.; Bolton, J. R. *J. Photochem. Photobiol., A-Chem.* **1999**, *128*, 1.

(44) Warneck, P.; Wurzinger, C. *J. Phys. Chem.* **1988**, *92*, 6278.

(45) Herrmann, H. *Phys. Chem. Chem. Phys.* **2007**, *9*, 3935.

(46) Honrath, R. E.; Peterson, M. C.; Guo, S.; Dibb, J. E.; Shepson, P. B.; Campbell, B. *Geophys. Res. Lett.* **1999**, *26*, 695.

(47) Dubowski, Y.; Colussi, A. J.; Hoffmann, M. R. *J. Phys. Chem. A* **2001**, *105*, 4928.

(48) Jones, A. E.; Weller, R.; Anderson, P. S.; Jacobi, H. W.; Wolff, E. W.; Schrems, O.; Miller, H. *Geophys. Res. Lett.* **2001**, *28*, 1499.

(49) Zhou, X. L.; Beine, H. J.; Honrath, R. E.; Fuentes, J. D.; Simpson, W.; Shepson, P. B.; Bottenheim, J. W. *Geophys. Res. Lett.* **2001**, *28*, 4087.

(50) Dubowski, Y.; Colussi, A. J.; Boxe, C.; Hoffmann, M. R. *J. Phys. Chem. A* **2002**, *106*, 6967.

(51) Boxe, C. S.; Colussi, A. J.; Hoffmann, M. R.; Tan, D.; Mastromarino, J.; Case, A. T.; Sandholm, S. T.; Davis, D. D. *J. Phys. Chem. A* **2003**, *107*, 11409.

(52) Chu, L.; Anastasio, C. *J. Phys. Chem. A* **2003**, *107*, 9594.

(53) Jacobi, H. W.; Annor, T.; Quansah, E. *J. Photochem. Photobiol., A-Chem.* **2006**, *179*, 330.

(54) Wingen, L. M.; Moskun, A. C.; Johnson, S. N.; Thomas, J. L.; Roeselová, M.; Tobias, D. J.; Kleinman, M. T.; Finlayson-Pitts, B. J. *Phys. Chem. Chem. Phys.* **2008**, *10*, 5668.

(55) Yu, Y.; Ezell, M. J.; Zelenyuk, A.; Imre, D.; Alexander, M. L.; Ortega, J.; Thomas, J. L.; Gogna, K.; Tobias, D. J.; D'Anna, B.; Harmon, C. W.; Johnson, S.; Finlayson-Pitts, B. J. *Phys. Chem. Chem. Phys.* **2008**, *10*, 3063.

(56) Raja, S.; Valsaraj, K. T. *J. Air Waste Manage. Assoc.* **2005**, *55*, 1345.

(57) Chen, J.; Ehrenhauser, F. S.; Valsaraj, K. T.; Wornat, M. J. *J. Phys. Chem. A* **2006**, *110*, 9161.

(58) Raja, S.; Valsaraj, K. T. *Atmos. Res.* **2006**, *81*, 277.

(59) Sumner, A. L.; Menke, E. J.; Dubowski, Y.; Newberg, J. T.; Penner, R. M.; Hemminger, J. C.; Wingen, L. M.; Brauers, T.; Finlayson-Pitts, B. J. *Phys. Chem. Chem. Phys.* **2004**, *6*, 604.

(60) Finlayson-Pitts, B. J.; Wingen, L. M.; Sumner, A. L.; Syomin, D.; Ramazan, K. A. *Phys. Chem. Chem. Phys.* **2003**, *5*, 223.

(61) Diamond, M. L.; Gingrich, S. E.; Fertuck, K.; McCarry, B. E.; Stern, G. A.; Billeck, B.; Grift, B.; Brooker, D.; Yager, T. D. *Environ. Sci. Technol.* **2000**, *34*, 2900.

(62) Gingrich, S. E.; Diamond, M. L. *Environ. Sci. Technol.* **2001**, *35*, 4031.

(63) Simpson, A. J.; Lam, B.; Diamond, M. L.; Donaldson, D. J.; Lefebvre, B. A.; Moser, A. Q.; Williams, A. J.; Larin, N. I.; Kvasha, M. P. *Chemosphere* **2006**, *63*, 142.

(64) Moussa, S. G.; McIntire, T. M.; Szori, M.; Roeselova, M.; Tobias, D. J.; Grimm, R. L.; Hemminger, J. C.; Finlayson-Pitts, B. J. *J. Phys. Chem. B* **2009**, *113*, 2060.

(65) Handley, S. R.; Clifford, D.; Donaldson, D. J. *Environ. Sci. Technol.* **2007**, *41*, 3898.

JP9070339